ACS Photonics

Letter

pubs.acs.org/journal/apchd5

All-Optical Method for Characterizing Individual Fluorescent Nanodiamonds

Benjamin T. Miles,[†] Alexander B. Greenwood,[†] Brian R. Patton,[‡] and Henkjan Gersen*[,†]

[†]Nanophysics and Soft Matter Group, H.H. Wills Physics Laboratory, University of Bristol, Bristol, BS8 1TL, United Kingdom

[‡]Centre for Neural Circuits and Behaviour, University of Oxford, Oxford, OX1 3SR, United Kingdom

ABSTRACT: Nitrogen-vacancy (NV^-) defects embedded in nanodiamond have attracted attention for their useful photonic and spin properties and their exceptional photostability. Efficiently detecting nanodiamonds that possess color centers and discriminating from any background fluorescent contamination are essential for nanodiamond-based technologies and thus necessitates the detection of both the nanoparticle and the fluorescent signature. However, optically detecting small nanodiamonds (<40 nm) proves difficult due to the low absorption and scattering cross section of nanodiamonds. Here we demonstrate an all-optical method capable of simultaneously colocalizing scattered signal from individual nanodiamonds (~10 nm) with the fluorescent signature from NV^- centers.

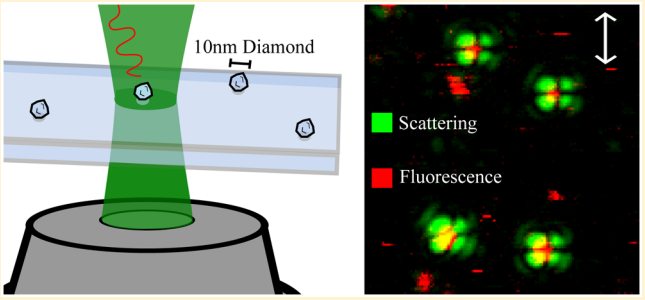

KEYWORDS: *cross-polarization imaging, nanodiamond, NV^- centers, single-particle detection, single-molecule detection, colocalization*

The applications for nanodiamonds (NDs) range from single-photon sources for quantum technologies,[1,2] to biocompatible, photostable trackers for biological labeling,[3,4] to nanosensing magnetic field probes for nuclear magnetic resonance spectroscopy.[5] However, these applications usually require that the selected NDs include a color center, an optically active defect in the diamond lattice, the most commonly desirable of which is a negatively charged nitrogen-vacancy (NV^-) defect. NV^- centers can be fabricated in NDs by ion bombardment to create defects that, followed by annealing, allow the color center to form by a diffusive process. The resultant defect is an extremely photostable emission center that acts as a single-photon emitter displaying quantum behavior up to room temperature.[6] To develop technologies that exploit these properties, it is essential that there is an effective and reliable method for identifying NDs that possess such NV^- centers. Moreover for their application in quantum technologies, a complete characterization of the individual or ensemble properties of the embedded color centers is required.

To characterize fluorescent nanoparticles such as nanodiamonds, one can employ techniques such as NSOM,[7−10] AFM,[11] TEM,[12] confocal microscopy,[13] or these tools in combination.[14] Regardless of the approach, it is important to correlate both the nanodiamond crystal and the fluorescent signature of any color center of interest in the same nanoparticle. This ensures that fluorescence arises from the NDs themselves rather than single molecules or other surface contaminants on the glass substrate, as was the case in a recent retraction of a quantum dot study published in *Nature*.[15] Ideally this two-component characterization is done rapidly using the same instrument to reduce ambiguity and the time taken to process the sample. However, when working with NDs, direct optical detection of the crystals below 40 nm diameter remains difficult due to the extremely low absorption cross section of diamond,[16,17] which prevents the use of particle detection techniques that rely on nonlinear absorption effects or photothermal heating. Recently, a group from Cardiff University showed highly effective detection of large ND crystals through coherent anti-Stokes Raman scattering, although the sensitivity of this process is limited to detecting NDs with a radius of >27 nm at the reported illumination powers and integration times.[14]

Motivated by this current limitation in the field, we apply our recently introduced technique, interferometric cross-polarization microscopy (ICPM), to the imaging of single NDs while simultaneously detecting the fluorescent signal from color centers. In doing so, we demonstrate an all-optical approach for the characterization of individual nanodiamond crystals containing NV^- centers. Furthermore, we achieve these detection sensitivities while using low excitation powers (25 μW on the sample) using an inexpensive laser system, in contrast to techniques such as four-wave mixing.[14] Operating at low powers enables the simultaneous detection of single-molecule fluorescence, making the technique an attractive option for rapidly identifying and rejecting fluorescent signal not originating from nanocrystals of interest. Furthermore, this makes the technique applicable to less photostable fluorophores or potentially to the study of shallow NV^- centers, which can also exhibit bleaching.[18]

ICPM[19] is an interferometric, point-scanning, confocal-like detection method with an optical sectioning capability on par

Received: December 18, 2015
Published: February 4, 2016

DOI: 10.1021/acsphotonics.5b00732
ACS Photonics 2016, 3, 343−348

with conventional confocal microscopy.[20] Due to operating in a crossed-polarized regime, the technique achieves detection sensitivities limited solely by the shot noise of the scattered signal and has demonstrated the detection of gold nanoparticles down to 5 nm at extremely low excitation powers (<1 μW), demonstrating its sensitivity.[19,21] Within the microscope, as schematically depicted in Figure 1a, a coherent laser source is

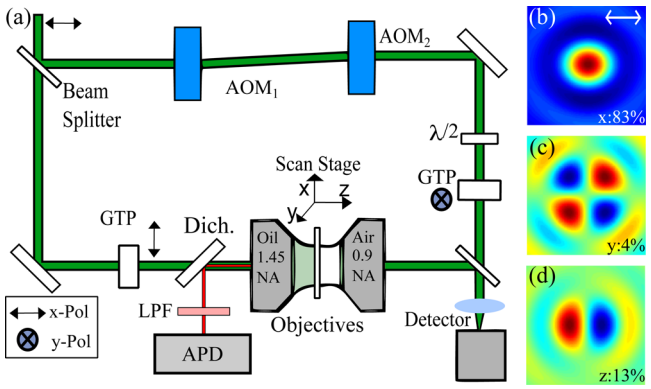

Figure 1. (a) Schematic diagram of interferometric cross-polarization microscopy (ICPM). A coherent source is split into frequency offset, orthogonally polarized signal, and reference paths enabling heterodyne detection of the scattered signal. Light in the signal branch is focused onto the sample by a high NA (1.45) objective, then recollimated by a second objective (NA 0.9) before recombining with the reference branch on a photodiode detector. (b–d) Strong focusing of linearly polarized light projects the polarization state across all three axes according to certain spatial distributions (1 μm × 1 μm). Only light scattered with like-polarization state to the reference path is interferometrically enhanced, producing the characteristic four-leaf-clover scattering distribution of ICPM.

incident on a 50:50 beam splitter to generate a signal and reference branch. To enable heterodyne detection, the reference branch is frequency offset by a pair of acousto-optic modulators before passing through a half-wave plate and a Glan–Thompson polarizer (GTP) oriented to produce *y*-polarized light. The signal branch is polarized by a second GTP to produce *x*-polarized light and focused via an oil immersion, high-numerical-aperture (NA 1.45) illumination objective onto a size 1.5H (Marienfeld) glass coverslip. The focused light is recollimated by a collection objective (NA 0.9) and overlapped with the reference branch by a second beam splitter, prior to focusing on a photodiode. The optical sectioning is defined by the interference of planar waves between the two branches; only light imaged from the focal region will interfere at the recombination beam splitter. Fluorescent signal is collected from the sample through the illumination objective and detected via a dichroic beam splitter (Semrock Di01-T405/488/532/647) on an avalanche photodiode (APD) with a dark count rate of less than 100 counts/second (PerkinElmer SPCM-AQRH-14).

According to the theory of strong electromagnetic focusing (the vectorial diffraction regime), a linearly polarized beam focused by high NA objectives projects a linear polarization state along all three axes, with a spatial and intensity distribution in the focal plane as seen in Figure 1b–d.[22−25] If undisturbed, the polarization distribution at the focus is retransformed into linear polarization by the collection objective, and no interferometric signal is detected on the photodiode, as interference does not occur between orthogonally polarized beams. In the case where an object with an electric dipole moment is present in the focus, light is scattered to the far field from all three polarization directions, proportionally to their representation in the focus and the dipole alignment. However, only forward scattered *y*-polarized light is interferometrically enhanced by the like-polarized reference branch, producing the signature four-leaf-clover scattering distribution observed when scanning a nanoparticle through the focus. This scattering distribution strongly reflects the corresponding component of the polarization at the focus (see Figure1c), albeit with the side lobes suppressed due to interference with a Gaussian reference beam.[21]

To prepare the ND sample, a coverslip is cleaned and surface charged by a 10 min 1:2 part sulfuric–nitric acid bath with two subsequent 10 min baths in double-deionized water. After diluting a solution of expected 20 nm diameter NDs, as purchased from Adámas Nanotechnologies, Inc., the NDs were drop deposited onto the coverslip, and after waiting 2 min excess solution was removed by exposure to a N_2 stream. To test both our deposition procedure and the size distribution of the deposited nanoparticles, the sample was imaged using AFM. A typical AFM image (3.5 × 2.5 μm area) is presented in Figure 2a. This demonstrates a size different from that quoted by the manufacturer, as we measure a mean height of 10 ± 2 nm with a low spatial concentration of larger particles as supported by a histogram of peak particle heights for 108 particles, Figure 2b. The interparticle distance observed is

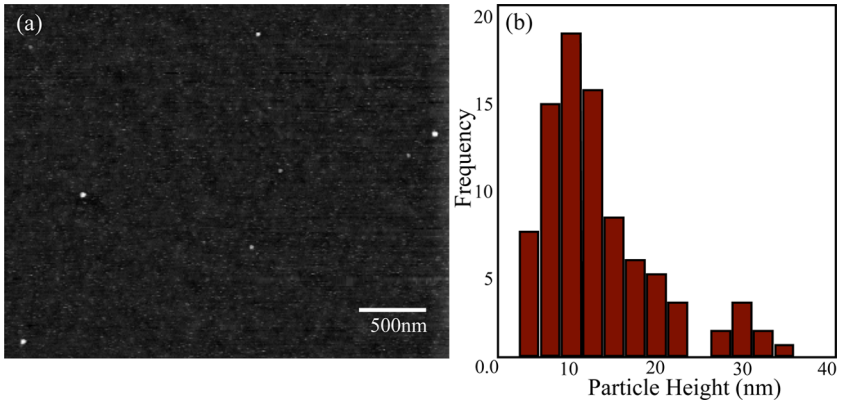

Figure 2. AFM image of a prepared ND sample (a) reveals a mean particle height of 10 ± 2 nm over a sample of 108 particles (b). By adjusting the dilution an average interparticle distance of 1 μm is achieved for optical imaging.

DOI: 10.1021/acsphotonics.5b00732
ACS Photonics 2016, 3, 343–348

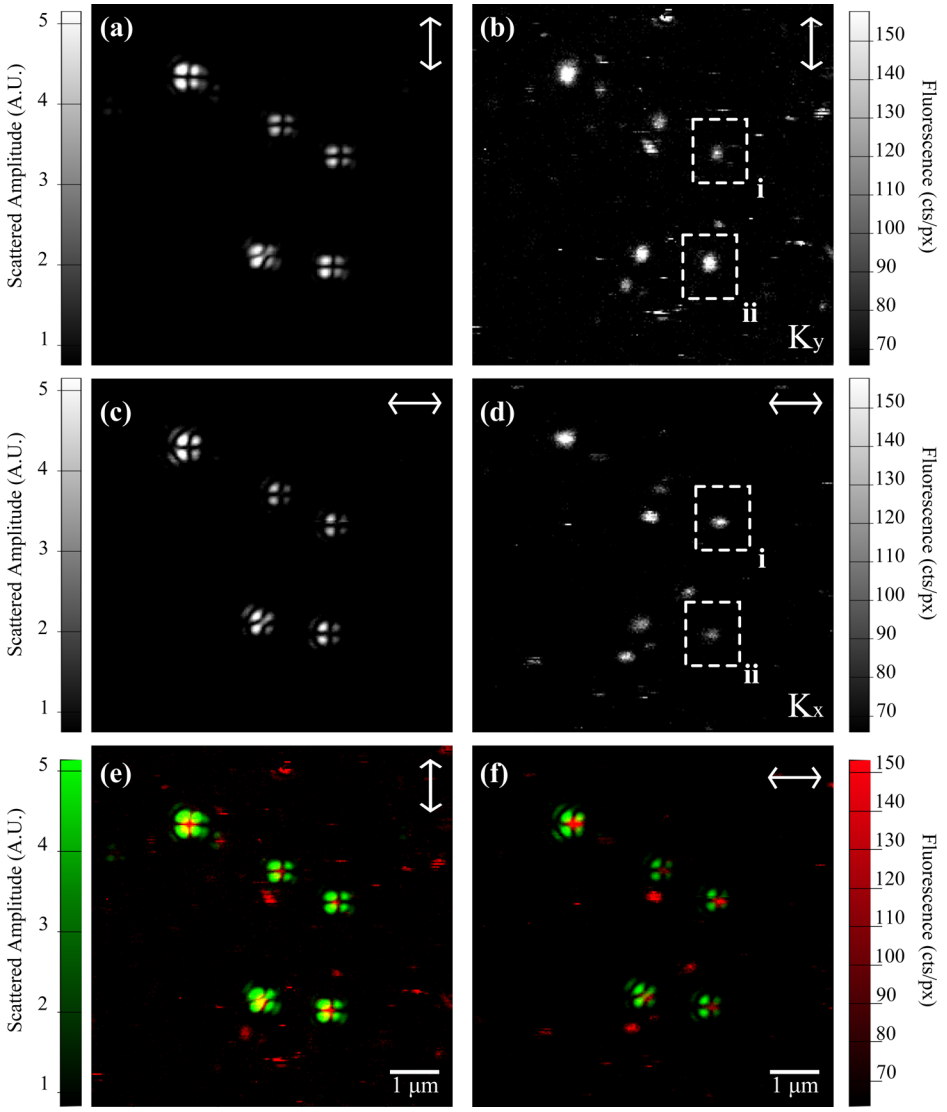

Figure 3. (a) A 532 nm illumination source is polarized in the *y*-direction, and an image of the scattered amplitude and (b) fluorescent signature of 10 ± 2 nm diamond nanoparticles is produced for 25 μW excitation power. The excitation polarization is then rotated to the *x*-direction, and the (c) scattered amplitude and (d) fluorescence are collected. The scattering and fluorescent data are assigned to the G and R channels of an overlaid image to show colocalization under (e) *y*-polarized and (f) *x*-polarized incident illumination.

typically >1 μm, as achieved by choice of solution concentration, ensuring the sample is sufficiently monodisperse to allow single particles to be imaged under a diffraction-limited approach.

A similarly prepared sample was imaged on the ICPM using an excitation wavelength of 532 nm while simultaneously collecting fluorescence on an APD with a 640 nm long pass filter. A typical image of the scattered optical amplitude as a function of position is shown in Figure 3a taken at 25 μW incident on the coverslip. The observed variation of peak intensities is consistent with the range of particle sizes observed under AFM as the scattered optical amplitude scales with D^3 in our approach. Here we clearly identify the characteristic four-leaf-clover scattering distribution associated with imaging under crossed polarization resulting from the field distribution in Figure 1c. A similar interparticle distance to the AFM data is observed, showing that it is indeed possible to detect 10 nm nanodiamond.

For an incident polarization direction along the *y*-axis, Figure 3b shows an example of the corresponding fluorescent image taken simultaneously to the scattering image in Figure 3a. Here we see an elongated diffraction-limited spot along the polarization direction in the fluorescent channel as expected from a strongly focused linearly polarized beam (Figure 1b). To probe the dipole nature of the NV^- center, which should absorb optimally when aligned with the polarization direction, a second image was taken with the incident and reference polarization rotated by 90 deg[23] (Figure 3c,d). Dashed boxes (i, ii) in Figure 3b,d highlight the fluorescent signature of two nanodiamonds that display peak fluorescence at 122 cts/px and 168 cts/px, respectively, under *y*-polarized illumination and 189 cts/px and 131 cts/px under *x*-polarized illumination. These trends, which are repeated over multiple images, indicate that there is preferred polarization alignment between particles for photon emission.[23] In this way, we can observe the dipolar behavior of individual NDs through colocalized detection between scattered and fluorescent signals at the single-molecule level.

False-color images for orthogonal polarization illuminations, Figure 3e,f, reveal that there is a fluorescent population, likely

DOI: 10.1021/acsphotonics.5b00732
ACS Photonics 2016, 3, 343−348

single fluorophores, without associated scattering objects, emphasizing the need for simultaneous detection of both particle and fluorescent signature. This fluorescent background is not observed when a sample is imaged following the same protocol without the ND solution, showing that this signal originates from the solution. The scattering signal in Figure 3f displays the first-order side lobes to the left of the cloverleaf consistently over all imaged particles. This is due to shifting the Glan−Thompson polarizer, which slightly changes the overlap between signal and reference path and, in principle, does not limit colocalization, as the scattered signal from Figure 3e can be used to colocalize against.

In our current work we are mainly interested in demonstrating an effective optical correlation technique for nanoparticles, with NV^- centers embedded in ND proving an excellent test case. We can determine the relative fraction of nanodiamond that contain NV^- centers, by measuring only two orthogonal excitation polarizations, as we will discuss shortly. Here, ICPM is configured to use linearly polarized beam paths for the high extinction ratios necessary for sensitive scattering detection,[21] although in principle it is possible to illuminate with circularly polarized light to optimally excite an NV^- center at arbitrary in-plane orientation. To fully characterize the 3D orientation of the NV^- center dipole moment, the incident polarization angle needs to be incrementally advanced through the full 2π phase space, or the NV^- center needs to be excited under radially polarized light;[26] this additional step is beyond the scope of this paper, but the required methodology is well established and will not pose a problem for future implementations of this technique as a characterization step for quantum devices.

To identify NDs with fluorescent color centers, a tracking algorithm is developed that utilizes the high detection sensitivity of scattered detection under ICPM to sample only particles that present a characteristic four-lobed scattering signal. This ensures that fluorescence signatures that arise from fluorescent molecules or other contaminants are not considered in the analysis, as all fluorescent peaks originating from an NV^- are required to colocalize well with a scattering object. For the amplitude component of the scattered signal, local scattering maxima are identified and grouped with all neighbors within 0.4 μm. Clusters of local maxima composed of exactly four maxima that also fit well to the spatial dimensions of the cloverleaf, as modeled in earlier works,[20] are considered singular scattering objects; all other scattered signals are rejected. To help eliminate clusters or false positives from nanoparticle contamination, scattering signals outside a window of expected amplitude responses may be removed.

Local maxima in the fluorescence data are located and paired to scattering particles by location, within a 0.1 μm tolerance of the center of the four-lobe pattern. In the case where no fluorescence signal can be colocalized with a scatterer, the average fluorescence value of the immediate area is assigned instead, which corresponds to the background fluorescence of the sample. The dipole-like behavior of an NV^- center is best described by a pair of degenerate orthogonal dipoles,[27] visualized as the x'- and y'-axes of an arbitrarily oriented coordinate system (x', y', z') in Figure 4. To remove the incident polarization direction dependence when aiming to colocalize scattered and fluorescent signals, a second image with incident polarization orthogonal to the first is therefore also collected. Fluorescent signatures from the orthogonal polarization image are similarly assigned to identified scattering objects after accounting for any small shift between subsequent measurements induced by rotating the Glan−Thompson polarizer.

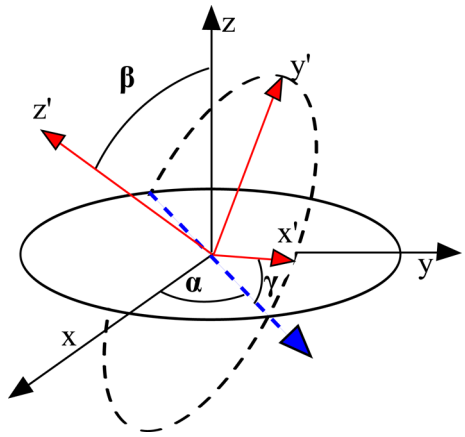

Figure 4. Dipole-like behavior of an NV^- center may be described as a pair of degenerate orthogonal dipoles.[28] A rotated coordinate system (x', y', z') (red) is defined relative to the laboratory frame (x, y, z) (black) in terms of Euler angles. For convenience, the two dipoles of an NV^- center are assigned with respect to (x', y', z') such that $\vec{\rho_1} = (1, 0, 0)$ and $\vec{\rho_2} = (0, 1, 0)$.

To combine these data sets, we consider the two degenerate orthogonal dipoles $(\vec{\rho_1}, \vec{\rho_2})$ of an NV^- center in terms of Euler angles with respect to the laboratory frame following Figure 4 as

$$\vec{\rho_1} = \begin{pmatrix} \cos(\alpha)\cos(\gamma) - \sin(\alpha)\cos(\beta)\sin(\gamma) \\ \sin(\alpha)\cos(\gamma) + \cos(\alpha)\cos(\beta)\sin(\gamma) \\ \sin(\beta)\sin(\gamma) \end{pmatrix} \quad (1)$$

$$\vec{\rho_2} = \begin{pmatrix} -\cos(\alpha)\sin(\gamma) - \sin(\alpha)\cos(\beta)\cos(\gamma) \\ -\sin(\alpha)\sin(\gamma) + \cos(\alpha)\cos(\beta)\cos(\gamma) \\ \sin(\beta)\cos(\gamma) \end{pmatrix} \quad (2)$$

For linearly polarized excitation, the polarized field at the focus is predominantly parallel to the light entering the illumination objective. Assuming both dipoles interact equally with an electric field,[27,28] for x-polarized excitation the fluorescent signal, K, can be shown to scale as

$$K_x = \sum_i^2 |\vec{\rho_i}\cdot\vec{E}|^2 = E_x^2[1 - \sin^2\alpha \sin^2\beta] \quad (3)$$

and for y-polarized excitation as

$$K_y = \sum_i^2 |\vec{\rho_i}\cdot\vec{E}|^2 = E_y^2[1 - \cos^2\alpha \sin^2\beta] \quad (4)$$

This allows for retrieval of $K(\beta)$, the fluorescence signal as a function of the projection of $\vec{\rho_1}$ and $\vec{\rho_2}$ onto the xy-plane, by summing the peak fluorescence signatures from two orthogonal polarization images under equal excitation powers, $|\vec{E}|^2$. The fluorescent signal from N NV^- centers is returned by the summation over all centers, following

$$K(\beta) = \sum_i^N [K_{xi} + K_{yi}] = \sum_i^N \vec{E}^2(1 + \cos^2\beta_i) \quad (5)$$

DOI: 10.1021/acsphotonics.5b00732
ACS Photonics 2016, 3, 343−348

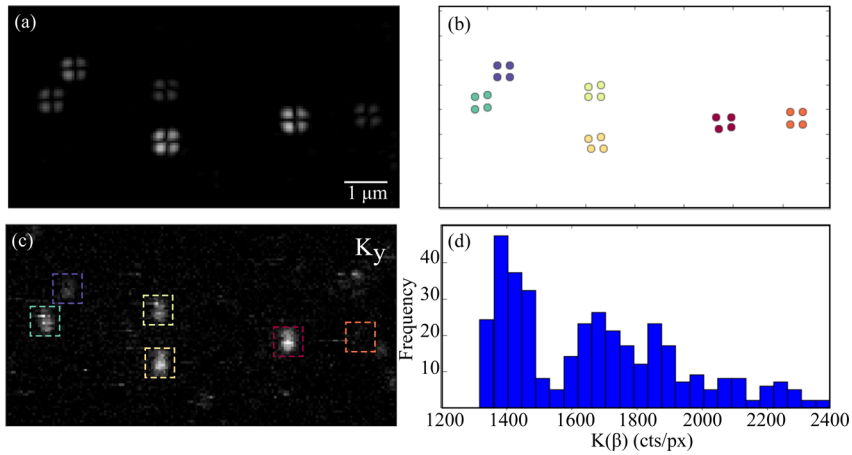

Figure 5. (a) Scattered amplitude image of 10 ± 2 nm diamond nanoparticles excited under 532 nm at 350 μW with (c) simultaneous detection of fluorescent signal. (b) Scattering maxima are locally grouped using the characteristic cloverleaf scattering signature to enable automated colocalization with fluorescent signatures so only fluorescent signatures with a corresponding scattering signal are considered. (d) Histogram of fluorescent counts, $K(\beta)$, as calculated for each scattering particle by the summation of two orthogonal polarization signals.

To properly characterize the nanodiamonds, we collect a large statistical data set by taking a series of images at 350 μW incident on the sample. This promotes bleaching of the observed background fluorophores in this specific sample and ensures sufficient excitation cycles of the NV^- center for a 2 ms pixel integration time to enable a fast scan time and minimal drift (40 μm × 40 μm, 700 px × 700 px, 1.6 s/line). Figure 5a shows a typical collection of particles where the tracking protocol has assigned local scattering maxima to clusters that fit well with the expected cloverleaf dimensions (b). The dashed areas in Figure 5c are a visual representation of the location of an expected corresponding fluorescent peak (K_y) for the scattering particles located in (a). The absence of a fluorescent signal for the right-most particle as well as an absence in the K_x image (not shown) is attributed to the presence of an ND without an NV^- center, allowing the ratio of fluorescence signal between particles with and without NV^- centers to be determined.

The histogram of fluorescent counts, $K(\beta)$, calculated following eq 5 is presented for all located scattering objects in Figure 5d. Where no fluorescent signature can be located from a scattering object, the local fluorescent background is averaged for a 0.4 μm^2 area centered at the scatterer's location in the fluorescent image, symbolically represented by averaging over the orange dashed box in Figure 5c. In this way, uncolocalized scattering objects effectively report on the average background fluorescent count rate of the sample. The peak located at $K(\beta)$ = 1400 cts/px corresponds to the average fluorescent background rate of the sample, where no fluorescent signature is located. The peak at K(β) = 1700 cts/px represents scattering signals that colocalize well with a defined fluorescent signal, which we assign tentatively to the presence of a single NV^- center based on the manufacturer's specifications (1−2NV^- centers per ND) and a discrete increase above the background fluorescence rate. However, it is worth noting that an ND containing two unfavorably aligned NV^- centers may also produce a similar signal level, although this population is expected to be small. Our approach could be extended to prove that these are indeed single NV^- centers by adding a second APD and time-correlated single photon counting module to enable a Hanbury Brown−Twiss (or antibunching) measurement. The collected fluorescence distribution can be understood from eq 5; there is an expected spread in the primary peak from variations in the β projection of the NV^- center and a tail to higher count rates likely resulting from the presence of multiple NV^- centers. Out of 408 particles analyzed, we find that 266 (65.12%) localize well with a fluorescent signal, a ratio the producer does not yet supply.

In conclusion, we have demonstrated an all-optical method to simultaneously resolve the scattering features of 10 ± 2 nm NDs and colocalize those with fluorescent signatures of NV^- centers. We observed good sensitivity even at low excitation powers (25 μW) despite the traditional limitation of optical observation due to the extremely small cross section of nanodiamonds. Additionally, the dipole-like behavior of NV^- centers was observed by excitation under orthogonal incident polarizations. The ability to verify the presence of color centers in individual particles is essential in the pursuit of using nanodiamonds in applications from quantum technologies to biological labeling.

AUTHOR INFORMATION

Corresponding Author

*E-mail: h.gersen@bristol.ac.uk.

Notes

The authors declare no competing financial interest.

ACKNOWLEDGMENTS

This work was funded in part by the Biotechnology and Biological Sciences Research Council through a Technology Development Research Initiative (grant ref BB/F004494/1) and a grant from the Engineering and Physical Sciences Research Council (grant ref EP/K502996/1), and carried out with the support of the Bristol Centre for Nanoscience and Quantum Information. B.R.P. is supported by a Royal Society University Research Fellowship.

REFERENCES

(1) Sipahigil, A.; Goldman, M. L.; Togan, E.; Chu, Y.; Markham, M.; Twitchen, D. J.; Zibrov, A. S.; Kubanek, A.; Lukin, M. D. Quantum Interference of Single Photons from Remote Nitrogen-Vacancy Centers in Diamond. *Phys. Rev. Lett.* **2012**, *108*, 143601.

DOI: 10.1021/acsphotonics.5b00732
ACS Photonics 2016, 3, 343−348

(2) Ladd, T. D.; Jelezko, F.; Laflamme, R.; Nakamura, Y.; Monroe, C.; O'Brien, J. L. Quantum computers. *Nature* **2010**, *464*, 45−53.
(3) Faklaris, O.; Garrot, D.; Joshi, V.; Druon, F.; Boudou, J.-P.; Sauvage, T.; Georges, P.; Curmi, P. A.; Treussart, F. Detection of single photoluminescent diamond nanoparticles in cells and study of the internalization pathway. *Small* **2008**, *4*, 2236−2239.
(4) Mohan, N.; Chen, C.-S.; Hsieh, H.-H.; Wu, Y.-C.; Chang, H.-C. In vivo imaging and toxicity assessments of fluorescent nanodiamonds in Caenorhabditis elegans. *Nano Lett.* **2010**, *10*, 3692−3699.
(5) Mamin, H.; Kim, M.; Sherwood, M.; Rettner, C.; Ohno, K.; Awschalom, D.; Rugar, D. Nanoscale nuclear magnetic resonance with a nitrogen-vacancy spin sensor. *Science* **2013**, *339*, 557−560.
(6) Schröder, T.; Schell, A. W.; Kewes, G.; Aichele, T.; Benson, O. Fiber-integrated diamond-based single photon source. *Nano Lett.* **2010**, *11*, 198−202.
(7) Sonnefraud, Y.; Cuche, A.; Faklaris, O.; Boudou, J.-P.; Sauvage, T.; Roch, J.-F.; Treussart, F.; Huant, S. Diamond nanocrystals hosting single nitrogen-vacancy color centers sorted by photon-correlation near-field microscopy. *Opt. Lett.* **2008**, *33*, 611−613.
(8) Drezet, A.; Sonnefraud, Y.; Cuche, A.; Mollet, O.; Berthel, M.; Huant, S. Near-field microscopy with a scanning nitrogen-vacancy color center in a diamond nanocrystal: A brief review. *Micron* **2015**, *70*, 55−63.
(9) Beams, R.; Smith, D.; Johnson, T. W.; Oh, S.-H.; Novotny, L.; Vamivakas, A. N. Nanoscale fluorescence lifetime imaging of an optical antenna with a single diamond NV center. *Nano Lett.* **2013**, *13*, 3807−3811.
(10) Eckert, R.; Freyland, J. M.; Gersen, H.; Heinzelmann, H.; Schürmann, G.; Noell, W.; Staufer, U.; De Rooij, N. F. Near-field fluorescence imaging with 32 nm resolution based on microfabricated cantilevered probes. *Appl. Phys. Lett.* **2000**, *77*, 3695−3697.
(11) Bradac, C.; Gaebel, T.; Pakes, C.; Say, J. M.; Zvyagin, A. V.; Rabeau, J. R. Effect of the Nanodiamond Host on a Nitrogen-Vacancy Color-Centre Emission State. *Small* **2013**, *9*, 132−139.
(12) Havlik, J.; Petrakova, V.; Rehor, I.; Petrak, V.; Gulka, M.; Stursa, J.; Kucka, J.; Ralis, J.; Rendler, T.; Lee, S.-Y. Boosting nanodiamond fluorescence: towards development of brighter probes. *Nanoscale* **2013**, *5*, 3208−3211.
(13) Yu, S.-J.; Kang, M.-W.; Chang, H.-C.; Chen, K.-M.; Yu, Y.-C. Bright fluorescent nanodiamonds: no photobleaching and low cytotoxicity. *J. Am. Chem. Soc.* **2005**, *127*, 17604−17605.
(14) Pope, I.; Payne, L.; Zoriniants, G.; Thomas, E.; Williams, O.; Watson, P.; Langbein, W.; Borri, P. Coherent anti-Stokes Raman scattering microscopy of single nanodiamonds. *Nat. Nanotechnol.* **2014**, *9*, 940−946.
(15) Wang, X.; Ren, X.; Kahen, K.; Hahn, M. A.; Rajeswaran, M.; Maccagnano-Zacher, S.; Silcox, J.; Cragg, G. E.; Efros, A. L.; Krauss, T. D. Retraction: Non-blinking semiconductor nanocrystals. *Nature* **2015**, *527*, 544.
(16) Colpin, Y.; Swan, A.; Zvyagin, A. V.; Plakhotnik, T. Imaging and sizing of diamond nanoparticles. *Opt. Lett.* **2006**, *31*, 625−627.
(17) Faklaris, O.; Joshi, V.; Irinopoulou, T.; Tauc, P.; Sennour, M.; Girard, H.; Gesset, C.; Arnault, J.-C.; Thorel, A.; Boudou, J.-P.; et al. Photoluminescent diamond nanoparticles for cell labeling: study of the uptake mechanism in mammalian cells. *ACS Nano* **2009**, *3*, 3955−3962.
(18) Schirhagl, R.; Chang, K.; Loretz, M.; Degen, C. L. Nitrogen-vacancy centers in diamond: nanoscale sensors for physics and biology. *Annu. Rev. Phys. Chem.* **2014**, *65*, 83−105.
(19) Hong, X.; van Dijk, E. M. P. H.; Hall, S. R.; Götte, J. B.; van Hulst, N. F.; Gersen, H. Background-free detection of single 5 nm nanoparticles through interferometric cross-polarization microscopy. *Nano Lett.* **2011**, *11*, 541−547.
(20) Miles, B. T.; Hong, X.; Gersen, H. On the complex point spread function in interferometric cross-polarisation microscopy. *Opt. Express* **2015**, *23*, 1232−1239.
(21) Miles, B. T.; Robinson, E. C.; Van Dijk, E. M.; Lindsay, I. D.; van Hulst, N. F.; Gersen, H. Sensitivity of Interferometric Cross-Polarization Microscopy for Nanoparticle Detection in the Near-Infrared. *ACS Photonics* **2015**, *2*, 1705−1711.
(22) Richards, B.; Wolf, E. Electromagnetic diffraction in optical systems. II. Structure of the image field in an aplanatic system. *Proc. R. Soc. London, Ser. A* **1959**, *253*, 358−379.
(23) Novotny, L.; Hecht, B. *Principles of Nano-optics*; Cambridge University Press, 2012.
(24) Bahlmann, K.; Hell, S. Electric field depolarization in high aperture focusing with emphasis on annular apertures. *J. Microsc.* **2000**, *200*, 59−67.
(25) Foreman, M. R.; Török, P. Computational methods in vectorial imaging. *J. Mod. Opt.* **2011**, *58*, 339−364.
(26) Dolan, P. R.; Li, X.; Storteboom, J.; Gu, M. Complete determination of the orientation of NV centers with radially polarized beams. *Opt. Express* **2014**, *22*, 4379−4387.
(27) Alegre, T. P. M.; Santori, C.; Medeiros-Ribeiro, G.; Beausoleil, R. G. Polarization-selective excitation of nitrogen vacancy centers in diamond. *Phys. Rev. B: Condens. Matter Mater. Phys.* **2007**, *76*, 165205.
(28) Hui, Y. Y.; Chang, Y.-R.; Mohan, N.; Lim, T.-S.; Chen, Y.-Y.; Chang, H.-C. Polarization modulation spectroscopy of single fluorescent nanodiamonds with multiple nitrogen vacancy centers. *J. Phys. Chem. A* **2011**, *115*, 1878−1884.

DOI: 10.1021/acsphotonics.5b00732
ACS Photonics 2016, 3, 343−348